A fuzzy decentralized algorithm for high-rise buildings subjected to seismic excitations

Y. Meng[1] , Z.Y. Chen[1], H. Wu[2] and Timothy Chen[3]

[1]School of Science, Guangdong University of Petrochemical Technology, Maoming, Guangdong, China; [2]School of Computer Science, Guangdong Polytechnic Normal University, Guangzhou, Guangdong, China and [3]Division of Engineering and Applied Science, Caltech, CA 91125, USA

Abstract

By the reason that mathematical analysis is not feasible for practical control of buildings, decentralized control (DC) and fuzzy control (FC) technologies were introduced to optimize the control problem of high-rise building (HRB) structures. For the control problem of HRB structures, magnetorheological fluid dampers (MRFDs) were introduced to optimize the lateral stress problem of each floor, and the influence of different output variables on FC was compared. In the analysis of fuzzy DC experiments, there were significant differences in the impact of different structural controls (SCs) on building acceleration. In the comparison of the interstory displacement (ISD) time history of the lower concrete structure, the maximum ISD value without control was -12 cm in the nineth second, -7 cm in the nineth second of LQR (linear quadratic regularization) control, and -6 cm in the FC. The proposed biomedical evolutionary technology had better SC effects in practical scenarios, with better safety and stability. The research was mainly based on FC controller technology, and in the future, updated IT2FL (interval type2 fuzzy logic) control technology can be adopted. At the same time, machine learning models are used to optimize parameter problems and improve the control effect of concrete structures. Therefore, fluid dampers help reduce vibrations caused by external earthquakes and other dynamic loads. By dampening devices, fluid dampers enhance the overall stability of the building by improving comfort levels. By allowing for lighter structural designs, fluid dampers can reduce the amount of material needed for construction, leading to cost savings. With reduced vibrations and stresses, there may be fewer maintenance issues over time. Fluid dampers can be designed for various types of structures and can be used in conjunction with other damping systems, making them flexible solutions for different engineering challenges. The future study can be effectively combined with base isolation systems to further improve a building's resilience against seismic forces.

CAMBRIDGE
UNIVERSITY PRESS

Introduction

High-rise buildings (HRBs) are defined as structures that typically exceed a height of around 75 feet (approximately 23 m) and often feature multiple stories, with some reaching hundreds of feet tall. These buildings are commonly used for residential, commercial, and mixed-use purposes. HRBs are characterized by their vertical design, which maximizes land use in urban areas where space is limited. HRBs are susceptible to vibrations caused by wind and seismic activity. Controlling these vibrations is essential to prevent discomfort for occupants and potential structural damage. Implementing effective damping systems, such as fluid dampers or tuned mass dampers, is necessary to mitigate motion and enhance comfort. Controlling concrete structures in HRBs presents unique challenges due to their height, complexity, and exposure to dynamic loads. Effective design, advanced materials, and innovative engineering solutions are essential to ensure the safety, stability, and comfort of these towering structures (Chen et al., 2024a; Xu et al., 2024, 2025a,b; Zhang et al. 2024b; Sun et al., 2025; Xie et al., 2025). Structural control (SC) refers to the techniques and systems employed to enhance the performance of structures against dynamic loads, such as wind, earthquakes, and vibrations. The primary goal is to minimize structural response, improve occupant comfort, and ensure safety. In HRBs, where the effects of these forces can be significant, effective SCs becomes critical (Tai et al., 2024; Wang et al., 2024a,b,d,f,h,i,k; Wu et al., 2024; Tang et al., 2025). Passive control systems include devices that absorb and dissipate energy from dynamic loads such as viscous dampers, friction dampers, and base isolation. It typically involves flexible bearings or pads. Active controls use sensors and actuators to actively counteract dynamic forces in real time. They adjust their response based on the detected motion of the building. Semiactive dampers combine passive damping elements with active control capabilities. They can adjust their properties (e.g., stiffness or damping) in response to external conditions without requiring a large energy input. Hybrid systems integrate multiple control strategies (e.g., combining passive dampers with active controls) to optimize performance across various loading conditions. Structural health

monitoring (SHM) utilizes sensors to continuously monitor the structural response of buildings. Data collected can inform control systems and provide early warnings for maintenance or repair needs. As technology advances, the integration of smart materials and monitoring systems will continue to enhance the effectiveness of SCs methods, ensuring that HRBs remain resilient and functional in the face of environmental challenges (Huang et al., 2022; Li et al., 2024; Long et al., 2024a,b; Qi et al., 2024; Shu et al., 2025). In summary, while SCs systems significantly enhance the performance and safety of high-rise buildings, their limitations—such as cost, complexity, and performance constraints—can pose challenges to constructing ever-taller HRBs. As technology continues to evolve, it may become more feasible to address these limitations, but for now, they do play a role in defining the practical height limits of high-rise construction.

Linear quadratic regulator (LQR) is widely used in control systems for specific reasons. LQR provides an optimal control strategy that minimizes a cost function, typically representing a trade-off between control effort and system performance (Lu et al., 2003; Gao et al., 2021; Gong and Li, 2024; Hu et al., 2024; Huang et al., 2024). LQR uses state feedback to determine the control input, which allows for a more precise control strategy since it takes the entire state of the system into account. The design of an LQR controller is mathematically straightforward and computationally efficient, especially for linear systems where it ensures system stability if the system is controllable and observable (Zhou et al., 2022, 2025; Cai et al., 2024; Chen et al., 2024d; Fu et al., 2024). Thus, LQR is favored in control systems due to its optimality, robustness, and flexibility, allowing engineers to design effective controllers for a variety of applications while ensuring system stability and performance (Yao et al., 2022; Yang et al., 2024a,b, 2025; Zhang et al., 2024a,b,c,e).

In the planning and design of concrete structures, it is necessary to consider the requirements of building project planning and structural risk requirements. The project planning requirements include design requirements such as the lifespan, applicability, and durability of the building. The risk of concrete structure mainly considers the safety risk, property loss, and social impact caused by structural damage. At present, the process of global city is accelerating, and HRBs are constantly rising. Compared with traditional low rise buildings, HRBs have outstanding advantages in land resource utilization, construction efficiency, and costs (Chen et al., 2024b). However, HRBs face significant structural risks that cannot be ignored. As the number of floors increases, the loads and various stresses borne by the building will continue to expand, and the safety risks faced by the building will also continue to expand. Earthquake vibration can cause serious crustal activity, causing significant impact and damage to HRB structures. Effective concrete structure control technology is of great significance for the safety of HRBs. At present, the control of concrete structures is mainly focused on the basis of overall control, and there is little research on the control of HRB structures. Therefore, research was conducted on HRB SC technology and the risks faced by different HRBSC technologies were analyzed. Fuzzy control (FC) and decentralized control (DC) technologies were introduced to optimize building control effects in different scenarios to meet the seismic safety requirements of HRBs. This study has important reference value for the optimization design of seismic resistant structures in HRBs.

In summary, FC and DC are emerging solutions in the field of SCs for HRBs. Both methods address some limitations of traditional control systems, offering potential advantages in managing dynamic loads and improving structural performance. DC refers to a control architecture where individual subsystems operate independently rather than relying on a central controller. Each subsystem can make decisions based on local information and conditions. FC and DC present promising alternatives to traditional SCs methods for HRBs. By addressing limitations such as cost, complexity, and adaptability, these approaches have the potential to facilitate the design and construction of taller, safer, and more resilient structures in the future. As research and technology in these areas advance, they may become integral components of modern structural engineering practices.

The research content is divided into four parts. The first part introduces relevant concrete structure control technologies and conducts research on specific application scenarios of FC and DC technologies. The second part is the study of FC theory and DC technology, to design a fuzzy-based concrete structure control unit and achieve optimal control of HRB structures. The third part is the application of FC technology in specific scenarios to verify the optimization effect of the proposed FC technology in SC of HRBs. The fourth part summarizes and analyzes the entire article and elaborates on the improvement direction of the research. This study has made the following important contributions in the field of HRBSC technology. First, it comprehensively considered the planning and structural risk requirements of building projects and clarified the safety, durability and applicability requirements that must be met in HRB design. Through in-depth analysis of these factors, the necessity and urgency of HRBSC technology were studied. Second, the introduction of FC and DC technologies has the potential to optimize the control effect of concrete structures in different scenarios. Through in-depth research on FC and DC technologies, a fuzzy-based concrete structure control unit has been established to achieve optimal control of HRB structures. It provides useful reference and inspiration for research in related fields and has high academic and practical application value.

Literature review of DC and FC

FC theory is widely applied in fields such as architecture, unmanned driving, and aerospace and is a type of intelligent control technology. The controller problem of nonlinear control systems described by fuzzy models was studied (Chen et al., 2024c). The developmental direction of modern manufacturing enterprises was proposed. On the basis of fuzzy theory, the relationship among the cost of product quality loss, the reliability of the assembly dimension chain, and assembly tolerance is studied together in this article. Processing cost can be considerably reduced, and the target of quality engineering is realized by optimization design. In this regard, an uncertain trigger variable method was proposed for the research of the system, which can design a new safety controller and meet the requirements of mismatched member functions. Through analysis, the proposed scheme had good security in practical applications. Several uncertain displacement response engineering examples to demonstrate the effectiveness and applicability with interval method and optimization algorithm were studied. Based on the mixed probability distribution model, the one-dimensional and two-dimensional interval load spectrum for shock absorber cylinder are established by analyzing the characteristics of load signals. In addition, based on the uncertain signal problems, the interval life spectrum and interval damage spectrum of one-dimensional and two-dimensional are constructed by the interval algorithm (Liu et al., 2022). And the model uses multiaxial fatigue test data to verify the validity and adaptability of the new model. The life prediction accuracy and

material application range are satisfactory. Research on decentralized ventilation systems in the field of architecture was conducted to ensure the exchange of fresh gases within the building. Aiming to provide comfortable and fresh ventilation strategies for buildings, a ventilation strategy based on fuzzy theory was proposed. This method has been compared with traditional controllers, and the proposed method could reduce energy by up to 12%. At the same time, a membership function has been added to the scheme, allowing customers to choose different service needs based on their own preferences. It was found that intelligent energy management systems have become an effective means of energy conservation in power grids, but this technology relied on predicting future dynamic factors. Aiming to better reduce electricity costs, a comprehensive prediction model was proposed, which was based on FC and time memory models to analyze and predict household electricity consumption at different time periods. At the same time, a fuzzy logic control unit was added to the entire system, which can facilitate people's better use of electrical equipment. Compared with traditional models, the proposed model could reduce household electricity costs at the optimal time and had excellent electricity scheduling performance. Research on existing building energy consumption and found that ventilation, heating, and air conditioning use account for a high proportion of building energy consumption was conducted. Effective building energy conservation strategies are crucial. Considering that building energy efficiency is influenced by many uncertain factors and cannot be monitored intuitively, a deep learning adaptive control technology for buildings was proposed. The goal of this technology was to reduce energy consumption while meeting comfort requirements. Fuzzy logic has been successfully implemented in adaptive cruise control systems to maintain safe distances between vehicles. FC is widely used in robotic navigation, allowing robots to make decisions in uncertain environments. A study on the current energy consumption of buildings was conducted, and it was necessary to fully consider the energy consumption situation of each project link during building construction to reduce project costs. So a population decision-making scheme was proposed, which used fuzzy theory to analyze evaluation information in uncertain environments. In swarm robotics, DC allows multiple robots to collaborate and perform tasks autonomously. DC systems manage HVAC operations in large buildings, allowing for independent zone control. FC and DC have found successful applications across various domains, demonstrating their effectiveness in managing complex systems. The cited references provide further insights into the implementation and advantages of these control strategies in real-world scenarios. Each method for controlling concrete structures has its strengths and weaknesses. Passive methods are simple and reliable but less effective under extreme conditions. Active and semiactive methods offer high adaptability and effectiveness but come with increased complexity and costs. Fuzzy logic and DC provide innovative approaches for managing uncertainty and local conditions but may require careful design and implementation. The choice of method depends on the specific requirements and constraints of the structural application.

The features of fuzzy logic—its ability to handle uncertainty, adapt to nonlinear systems, incorporate expert knowledge, and provide real-time processing—make it a powerful tool for controlling various aspects of buildings. These characteristics enhance operational efficiency, user comfort, and overall building performance, aligning well with modern smart building technologies. The proposed technology mainly utilized magnetorheological damper technology and established an adaptive collaborative control

strategy for vibrating buildings under changes in stiffness and viscosity coefficient through Lyapunov stability analysis. At the same time, to improve the adaptability of the technology, ASC control law and adaptive law strategies were adopted. Finally, the effectiveness of the proposed method was verified and evaluated through numerical simulation, and the results showed that the building had good seismic control effect under earthquake action, while reducing the impact of earthquake damage. DC presents numerous advantages, including scalability, resilience, faster response times, and reduced communication loads. These features make it particularly suitable for complex, dynamic environments such as smart buildings, transportation systems, and networked infrastructures, where adaptability and reliability are crucial. At the same time, an adaptive control technology was proposed by combining adaptive back control and Lyapunov stability theory. Through implementation, the state variables in the closed-loop system had stability, and this control technology had good application effects. Research on feedback DC technology was conducted, which required the presence of unknown and indescribable states in the system. They conducted modeling research on fuzzy logic position scores. At the same time, an adaptive backstepping control strategy was introduced to obtain a new control strategy. It verified the proposed scheme, which could ensure good stability and control effect of the system, and had good application effect in concrete structure control.

Based on the above research, FC theory and decentralized adaptive control system have important applications in the field of intelligent control. However, the vibration control of HRB structures is complex and unpredictable, and there is relatively little research in this field in the relevant literature. At the same time, there is relatively low research on the dispersion of HRBs in relevant literature. In this regard, the introduction of FC and DC systems in the vibration control of HRB structures is aimed at improving the safety of HRB structures under vibration conditions, providing technical reference for structural design optimization of HRBs.

Construction of concrete structure vibration control model based on FC algorithm

At first, the number of degrees of freedom of a concrete structure is defined as n, which is subjected to seismic excitation. For the convenience of control, a shear model is used to construct floor parameters as shown in Figures 1 and 2.

This section mainly analyzes FC and DC technologies, applies them to the field of HRB SC, and constructs a building SC model. At the same time, it analyzes the types of concrete structure control, constructs a magnetorheological fluid damper (MRFD) control model, and applies it to specific multifloor concrete structure control fields.

Concrete structure based on fuzzy DC

The traditional centralized control scheme cannot meet the stability and seismic requirements of HRB structures. DC scheme and FC technology are utilized to obtain structural risks in HRBs, thereby improving the stability and safety of HRB structures. Traditional centralized control schemes face significant challenges in maintaining stability due to their reliance on a single controller, communication delays, lack of local adaptation, and difficulties in managing complex, nonlinear systems. These limitations can lead to

vulnerabilities, inefficiencies, and instability, particularly in dynamic and large-scale environments. DC approaches often provide a more robust solution by distributing decision-making and enhancing system resilience. The equilibrium motion model of the building is shown in Eq. (1).

$$\begin{cases} M\ddot{X}(t) + C\dot{X}(t) + KX(t) = D_sF(t) + B_sU(t) \\ X(t_0) = X_0, \dot{X}(t_0) = \dot{X}_0 \end{cases} \quad (1)$$

In Eq. (1), K, C, and M all represent the building stiffness, damping matrix, and building mass, respectively; $X(t)$ means the building displacement vector; D_s denotes the external interference matrix; $U(t)$ expresses the actuator control vector; $F(t)$ indicates the external excitation vector; B_s refers to the actuator positioning matrix; $X(t_0)$ stands for the initial displacement of the structure; and $\dot{X}(t_0)$ means the initial velocity vector of the structure. In the analysis of concrete structure models, if the vibration damping ratio parameter of the first period of the concrete structure is set to 2%, and the remaining periods are all below 10%. The expression of the vibration damping ratio in the first period is shown in Eq. (2).

$$\xi_i = min\left\{\frac{\omega_i}{50\omega_1}, 0.1\right\} \quad (i = 2, \cdots, n) \quad (2)$$

At this moment, the damping matrix is expressed as shown in Eq. (3).

$$C = M\Phi\Lambda[2\xi_1\omega_1, 2\xi_2\omega_2, \cdots, 2\xi_n\omega_n]\Phi^{-1} \quad (3)$$

In Eq. (3), Φ denotes the formation matrix; ξ_i is the damping ratio of the i period; ω_n indicates the natural frequency of the i period. The concrete structure equation is shown in Eq. (4).

$$\begin{cases} \dot{Z}(t) = AZ(t) + BU(t) + DF(t) \\ Z(t_0) = Z_0 = \begin{bmatrix} X_0 \\ \dot{X}_0 \end{bmatrix}_{2n \times l} \end{cases} \quad (4)$$

In Eq. (4), A, B, and D are expressed as shown in Eq. (5).

$$\begin{cases} A = \begin{bmatrix} 0_{n \times n} & I_{n \times n} \\ -M^{-1}K & -M^{-1}C \end{bmatrix}_{2n \times 2n} \\ B = \begin{bmatrix} 0_{n \times p} \\ M^{-1}B_s \end{bmatrix}_{2n \times p} n \times \\ D = \begin{bmatrix} 0_{n \times q} \\ -\{1\} \end{bmatrix}_{2n \times q} \end{cases} \quad (5)$$

In Eq. (5), $M^{-1}K = \Phi$ refers to the formation matrix; $0_{n \times n}$, $0_{n \times p}$, and $0_{n \times q}$ express the $n \times n$, $n \times p$, and $n \times q$ dimensional zero matrix; B_s stands for the actuator displacement matrix; and $I_{n \times n}$ expresses the identity matrix. Distributed structure control system is different from centralized structure system control. The internal structure of a distributed system is composed of multiple substructure systems, each of which has an independent controller and can perform separate SC based on the concrete structure. The principle is shown in Figure 1. Parallel DC is a control strategy where multiple independent controllers operate simultaneously to manage different subsystems or components within a larger system. Each controller makes decisions based on local information and
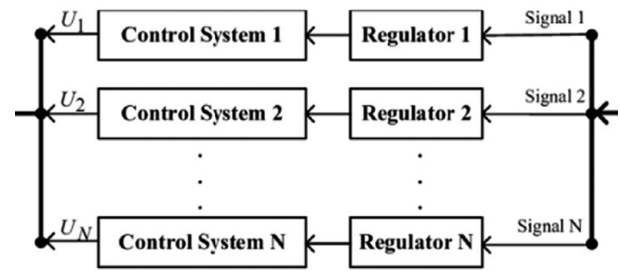

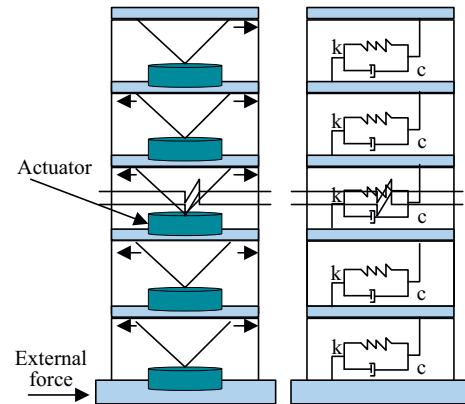**Figure 1.** Schematic diagram of decentralized control structure.

Figure 2. Schematic diagram of actuator arrangement.

conditions, allowing for real-time responses and enhanced system performance.

The subsystems of the DC system will effectively control based on the data conditions of the structural layer and form a complete closed-loop SC system. The unpredictability of HRB control characteristics arises from a combination of dynamic environmental conditions, complex structural interactions, human activities, and limitations in control systems. Understanding and mitigating these factors are crucial for enhancing the reliability and safety of HRBs. The choice between precise mathematical and analytical solutions depends on the problem at hand. For complex systems where analytical solutions are not feasible, precise mathematical methods are often better. Conversely, when an analytical solution exists, it can provide valuable insights and exact results. In many cases, a combination of both methods can be beneficial—using analytical solutions to gain insights and validate numerical results from precise mathematical approaches. Therefore, FC technology is introduced to determine SC parameters. The fuzzy domain set is defined as U, and its expression is shown in Eq. (6).

$$U = \{u_1, u_2, \cdots u_n\} \quad (6)$$

In Eq. (6), $u_1, u_2, \cdots u_n$ indicate the domain set. In FC, the selection of membership function will affect the overall effectiveness of FC, and the membership function suitable for FC will be ultimately obtained through empirical, subjective, and objective data support. The membership function is determined by fuzzy statistics, and the variable set of cloud top boundary belonging to the set U is defined as A^*. The element u_i of the subtest subset in n belongs to A^*, which is expressed as $n_{\dot{A}}$. A stable $n_{\dot{A}}/n$ ratio can be obtained through multiple experiments, and then u_i belongs to the fuzzy set A membership, which is expressed in Eq. (7).
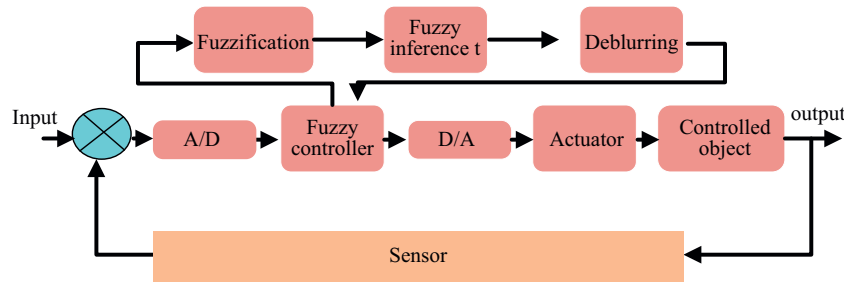
Figure 3. Schematic diagram of the fuzzy control system structure.

$$\mu_A(u_i) = \lim_{n \to \infty} \frac{n_{\dot{A}}}{n} \tag{7}$$

In Eq. (7), A denotes the borderless and $A^{\cdot}$ consistent fuzzy set; n means the amount of tests; u_i represents the amount of $u_i \in A^{\cdot}$ in the n test. The FC system is shown in Figure 3.

In Figure 3, the FC part mainly uses the maximum membership function method to determine accurate control values. This method is convenient and simple and is suitable for the field of concrete structure control. By processing the externally received analog signal through FC, it is converted into digital information in real time and transmitted to the sensor to achieve a dynamic control effect. The data rates of sensors can range from very low (1 Hz) for simple measurements to several kHz for complex applications such as LIDAR and cameras. The choice of sensor and its data rate often depends on the specific application requirements, including the need for real-time processing and the type of information being captured. In specific FC, due to the fact that different inference results in fuzzy reasoning correspond to different degrees of membership, the maximum one of these degrees of membership is used as the output, as shown in Eq. (8).

$$u_0 = \max \mu_A(u) \quad u \in U \tag{8}$$

In the process of fuzzy reasoning, there are multiple outputs corresponding to the max membership degree, and the mean of all corresponding values is selected as the final output value, as expressed in Eq. (9).

$$u_0 = \frac{1}{J} \sum_{j=1}^{J} u_j \tag{9}$$

Among them, u_j and J are expressed as shown in Eq. (10).

$$\begin{cases} u_j = \max_{u \in U}(\mu_A(u)) \\ J = |\{u\}| \end{cases} \tag{10}$$

FC with magnetorheological fluid damper

In the field of concrete structure control, traditional semiactive control strategies cannot meet the requirements of fast and short response changes during earthquakes, and earthquake adjustment parameters can be calculated in a relatively short time. The fuzzy DC technology is applied to the magnetorheological fluid damper (MRFD), which is widely used in the field of concrete structures. It has the advantages of low energy consumption, fast response, and can be combined with microcomputer control technology. The
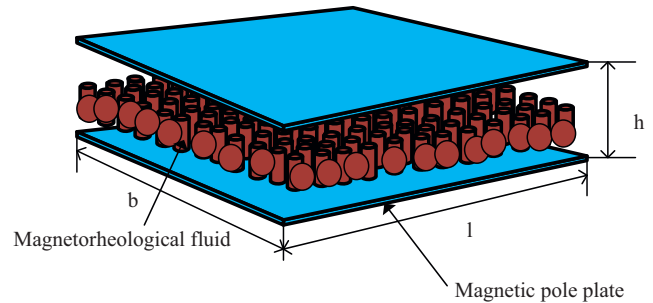

Figure 4. Schematic diagram of the motion state of magnetorheological fluid damper with two parallel plates.

motion state diagram of the MRFD with two parallel plates is shown in Figure 4.

According to the constitutive equation of magnetic current in the stable shear field, this state can be described, as shown in Eq. (11).

$$\tau = \tau_y \, sgn(\dot{y}) + \eta \dot{y} \tag{11}$$

In Eq. (11), τ_y denotes the yield of the magnetorheological fluid; τ means the total shear stress of the magnetorheological fluid; and $\dot{y}$ refers to the parameters of the magnetized fluid. When the particles do not meet magnetic saturation, the shear yield under the theory of magnetorheological fluid is expressed in Eq. (12).

$$\tau_y = \sqrt{6} \phi \mu_0 M_s^{1/2} H_0^{2/3} \tag{12}$$

In Eq. (12), M_s stands for the magnetization intensity of the saturated particle state; ϕ means the particle content of the magnetorheological fluid; μ_0 refers to the true permeability; and H_0 represents the applied magnetic field intensity. In the entire study of MRFD, their structure is mainly composed of a cylinder body, a piston, a magnetic fluid variant, and an electromagnetic coil. Taking the common shear valve-type MRFD as the object of study, it can be considered a valve-type damper and shear damping force, as expressed in Eq. (13).

$$F = \left[\frac{3\pi\eta L(D^2 - d^2)}{4Dh^3} + \frac{L\pi D\eta}{h} \right] v + \left[\frac{3\pi L(D^2 - d^2)}{h} + L\pi D \right] \tau_y sign(v) \tag{13}$$

In Eq. (13), η stands for the apparent density of the magnetorheological fluid; $sign(v)$ indicates the piston motion control function; h means the particle gap of the magnetorheological fluid; D means the

piston diameter; d refers to the internal diameter of the piston; and L stands for the effective length of the piston. According to Eq. (12) and Eq. (13), the shear-type MRFD model can be simplified, as shown in Eq. (14).

$$F_{sv} = \frac{3\eta L\left[\pi\left(D^2 - d^2\right)\right]^2}{4Dh^3}v + \frac{3L\pi\left(D^2 - d^2\right)}{4h}\tau_y\, sgn(v) \quad (14)$$

According to Eq. (14), the model is composed of two terms. The first term mainly considers fluid power viscosity, which is a fixed value. In the second item, the yield strength of magnetorheological fluid is mainly considered, which is related to variable Coulomb damping. Therefore, the adjustable multiple of MRFD is shown in Eq. (15).

$$\beta_v = \frac{bh^2\tau_y}{4\eta Q} = \frac{Dh^2\tau_y}{\eta\left(D^2 - d^2\right)v} \quad (15)$$

In Eq. (15), v denotes the piston speed and b expresses the Coulomb damping characteristic parameter. By adjusting the effective length and damping force of the piston appropriately, the SC adaptability of the damper can be changed. However, in practical control, the relationship between damping force and adjustable multiple is contradictory, and it is necessary to fully consider the actual needs of the concrete structure to meet the seismic control requirements of the concrete structure. At the same time, it is necessary to control strategies, and the selection of control strategies will directly affect the control effect of MRFD on concrete structures. In the research, fuzzy DC strategy is mainly used and compared with traditional LQR control strategy. LQR can obtain the optimal control law with linear feedback of the state, which makes it easy to form closed-loop optimal control. LQR optimal control can achieve good performance indicators of the original system at a low cost.

The MRFD action position matrix is defined as B_s, and MRFD dampers are arranged between two adjacent floors. The control drive is labeled as $u_j(t)$, the forward force applied to the j layer is marked as $u_j(t)$, and the reaction force applied to the $j-1$ layer is denoted as $-u_j(t)$. The control model is expressed in Eq. (16).

$$B_s U(t) = -C_d\dot{X} + B_s U_{sy} \quad (16)$$

In Eq. (16), B_s means the actuator positioning matrix; C_d indicates the viscous damping coefficient; U_{sy} refers to the damping control force vector; $U(t)$ stands for the SC force; and $\dot{X}$ expresses the relative velocity of the damper movement. The entire fuzzy DC principle is shown in Figure 5.

Multifloor fuzzy DC with LQR

Comparing DC and centralized control helps in understanding their respective strengths and weaknesses, enabling the selection of the most appropriate control strategy based on specific system requirements, complexity, and operational goals. At present, HRBs mainly rely on DC, and each controller is independent of each other to achieve adaptive control of complex environments in HRBs. In the DC of HRBs, the more controllers are divided into different floors, the better the control effect, but the lower the economic efficiency is. Therefore, it is necessary to fully consider the actual situation of the floors. DC is the division of floors into multiple floor control units, which are controlled independently of each other. Due to the higher the floor, the higher the uncertainty factor of the floor, and the more floor structure control parameters are required, an additional FC controller is designed in each floor structure control. In the research, the actuator adopts a direct drive form and has good performance in current HRBSC. The positioning moment of the actuator is shown in Eq. (17).

$$B_s = \begin{bmatrix} 1 & 0 & 0\ldots0 \\ 0 & 1 & 0\ldots0 \\ \vdots & \vdots & \vdots \ddots \vdots \\ 0 & 0 & 0\ldots1 \end{bmatrix}_{n\times n} \quad (17)$$

In the control of HRB structures, it is usually necessary to consider the effects of building mass, vibration acceleration, and other factors on concrete structure control. In this regard, each domain is divided into seven fuzzy subsets, including seismic acceleration, interlayer displacement, and so on, corresponding to one to seven top-level discrete controls, namely negative big, negative medium, negative small, zero, positive small, positive medium, and positive big. NB, NM, NS, ZE, PS, PB, and PB represent seven levels. The control coefficient is opposite to the domain name, and the maximum control force in concrete structure control can be controlled through a proportional factor. Based on the experience of membership selection introduced in the following section, the interlayer displacement, seismic acceleration, and control force are plotted as membership function curves. The acceleration membership function curve is shown in Figure 6.

The function of FC is that when the concrete structure is faced with seismic action and the acceleration is PB corresponding to the interstory displacement (ISD), the floor is in the most unfavorable seismic state, and the building seismic hierarchy of hazard controls is the largest at this moment. When the acceleration level under seismic excitation is NB, and the ISD level of the building is PB, the
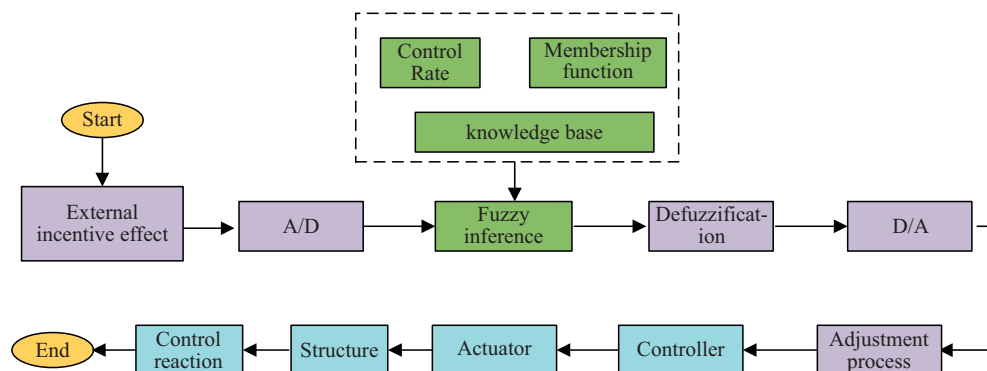

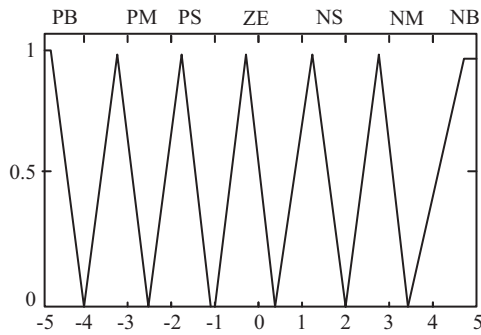**Figure 5.** Schematic diagram of fuzzy decentralized control process.

Figure 6. Acceleration membership relationship.

Table 1. Fuzzy control rules table

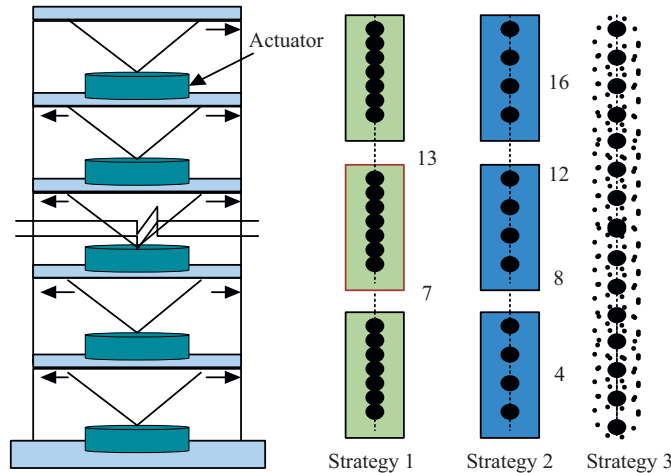| x\a	NB	NM	NS	ZE	PS	PM	PB
NB	7	6	5	4	3	2	1
NM	6	5	4	3	2	1	2
NS	5	4	3	2	1	2	3
ZE	4	3	2	1	2	3	4
PS	3	2	1	2	3	4	5
PM	2	1	2	3	4	5	6
PB	1	2	3	4	5	6	7

Figure 7. Schematic diagram of decentralized control strategy.

ISD is opposite to the seismic acceleration, the corresponding building hierarchy of hazard controls is the smallest, and the concrete structure control is the safest. The corresponding hierarchy of FC is shown in Table 1.

The maximum control force of the floor is set to *5 m/s²* × 1.1×10^6 *kg* = 5.5×10^6 *N*. In fuzzy DC, concrete structure control is mainly divided into multiple sub-SC units, and different structural units can adopt different control strategies. Figure 7 shows the three strategies used in fuzzy DC.

In the entire concrete structure control, three SC strategies are adopted. In SC strategy 1, the model is divided into three subcontrol units: first to seventh floors, eighth to 14th floors, and 15th to 20th

floors. In SC strategy 2, according to the characteristics of the floor structure, it is divided into 5 subcontrol units: first to fourth floors, fifth to eighth floors, nineth to 12th floors, 13th to 16th floors, and 17th to 20th floors. In SC strategy 3, it belongs to completely DC, where actuators are set in each layer and an FC controller is set in the single-layer unit structure to achieve SC of the entire building. At the same time, in the control of multifloor concrete structures, considering that the FC controller has a relatively average effect in concrete structure control, if the actuator acts on the interlayer, the FC controller relies on empirical data and cannot meet the control requirements. For this issue, the application of layer MRFD in multifloor structure control will be investigated to achieve effective control.

Suppose that we have a stabilizable full-order model in Eq. (5) to minimize the performance index

$$J = \int_0^\infty \left[X^T(t) Q_c X(t) + U^T(t) R_c U(t) \right] dt$$

where $Q_C = Q_C^T = H^T H \geq 0$ (positive semidefinite) and $R_C = R_C^T > 0$ (positive definite). This performance index, commonly called quadratic performance index, says that we wish to find an optimal control law $U^*(t)$ such that the integral-squared-error of the deviations of the state trajectories from the nominal is kept small without using a great deal of control energy. The weighting matrices Q_C and R_C are chosen by the designer to dictate the relative importance of the states and control energy. Without going into the optimization theory required to prove what the solution is, we simply claim that a unique optimal control law that minimizes J exists and is given by (Lu et al., 2003).

$$U^*(t) = R_c^{-1} B^T P_c X(t) = K_c X(t)$$

where P_C is a constant, symmetric, positive semidefinite matrix which is the solution to the algebraic Riccati equation.

$$A^T P_C + P_C A - P_C B R_C^{-1} B^T P_C + Q_C = 0.$$

The closed-loop regulator is asymptotically stable and the minimum value of J is $X^T(0) P_C X(0)$.

Example of DC in vibration control

This section mainly verified the proposed fuzzy SC technology, which mainly tested parameters such as interlayer displacement and building acceleration under seismic excitation, to evaluate the effectiveness of SC technology. Before the simulations, Figure 8 shows the flow chart representing the process of an industry-standard experimental model for controlling the vibration of buildings. This flow chart outlines the key steps in the experimental model for controlling vibrations in buildings without using a shake table, focusing on model construction, sensor installation, testing, and analysis.

FC based on MRFD

To verify the FC effect of MRFDs, a concrete structure benchmark model platform was selected for relevant experiments. The benchmark model platform for concrete structure was selected for relevant experiments. The experiment followed the American construction industry standard of a 20-story seismic resistant steel structure building as the experimental model. Assuming that the horizontal stiffness of the floor slab is infinitely large, the horizontal
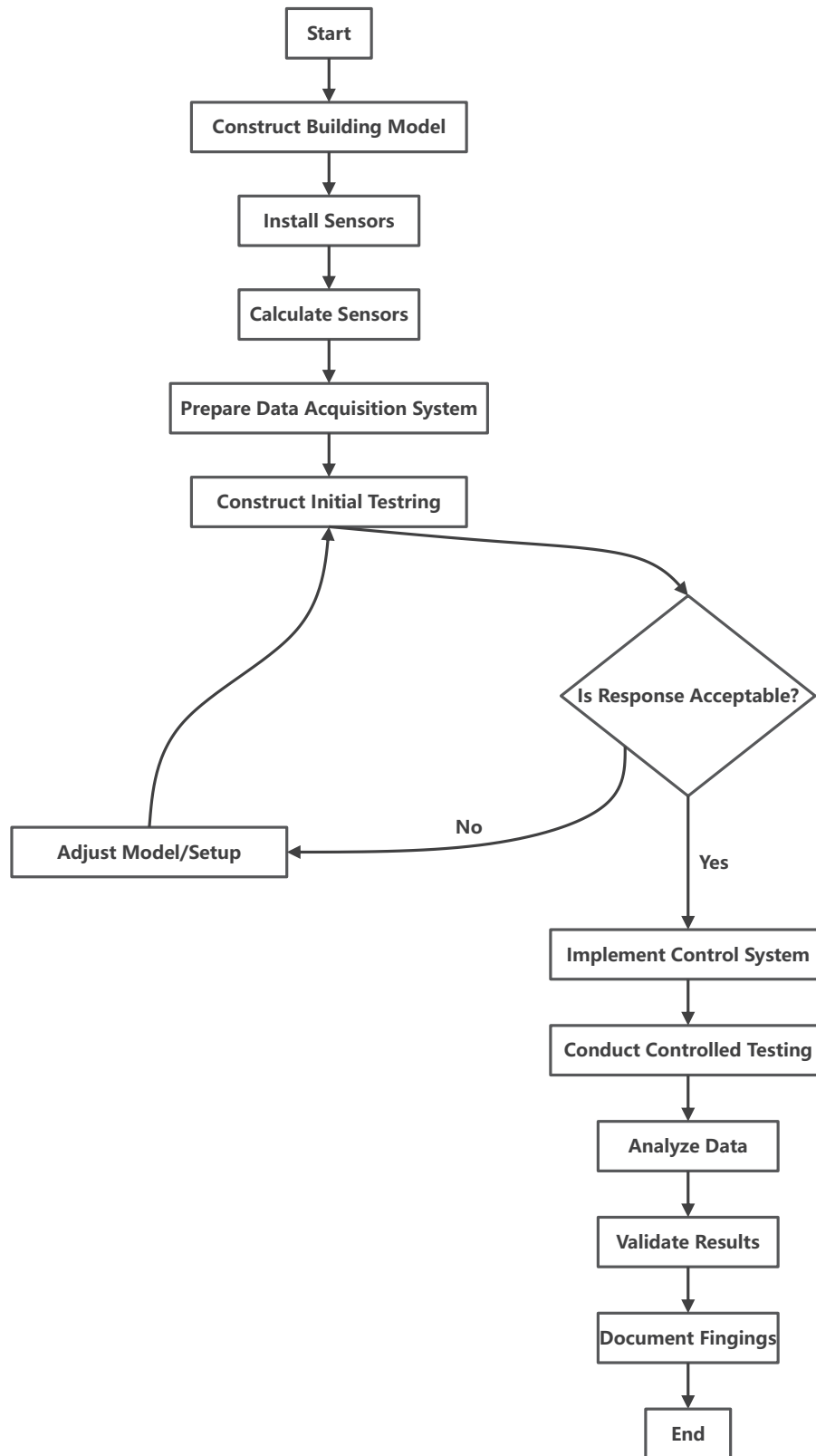
Figure 8. Flow chart of industry-standard experimental model for controlling the vibration of buildings.

and lateral stiffness between floors were preserved. In the experiment, only the vertical impact of earthquake was considered, and the vertical freedom of the frame was not studied. At the same time, to better analyze the seismic effect of concrete structures, without considering the influence of rotational degrees of freedom, a shear model was adopted for experiments. Meanwhile, when selecting seismic signals, FEMA guidelines should be followed. Table 2 shows the basic data of the benchmark building model.

Table 2. Basic data of benchmark architectural model

Number of layers	Quality, m (×10 kg)	Stiffness, k (×10 kN/m)
First floor	1.126	862.07
Second to fifth floor	1.100	862.07
Sixth to 11th floor	1.100	554.17
12th to 14th floor	1.100	453.51
15th to 17th floor	1.100	291.23
18th to 19th floor	1.100	256.46
20th floor	1.170	171.70
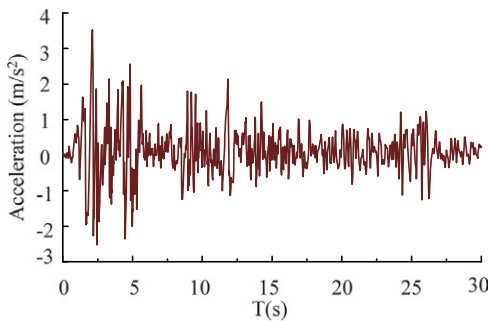
(a) El seismic waveform
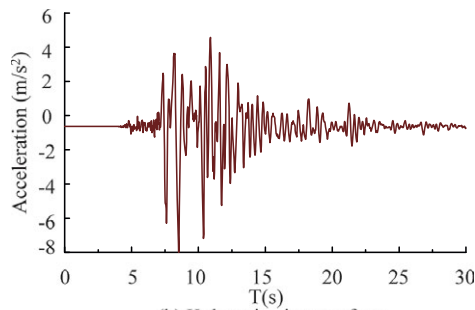
(b) Kobe seismic waveform

Figure 9. Acceleration curves of two types of seismic waves.
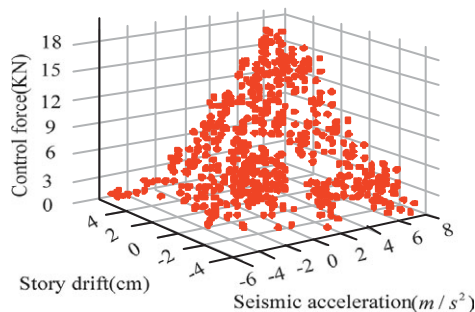

Figure 10. Relationship between structural control force, interlayer displacement, and seismic acceleration.

In the experiment, two types of seismic excitation waves were selected to simulate the SC effect, one being El Centro wave and the other being Kobe wave, with accelerations of 3.42 and 8.18 m/s², respectively. And it was compared with the traditional LQR structure control technology to verify the actual application effect of the research technology. Figure 9 shows the curves of two types of waves.
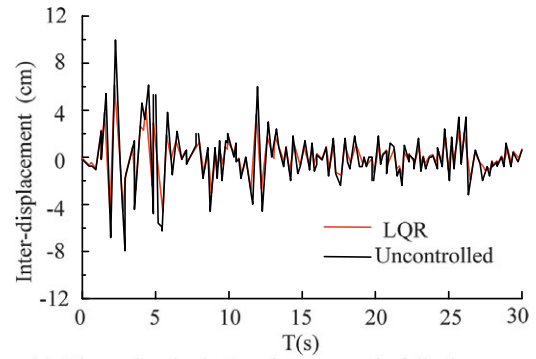
(a) Linear Quadratic Regulator control of displacement time history curve between lower layers
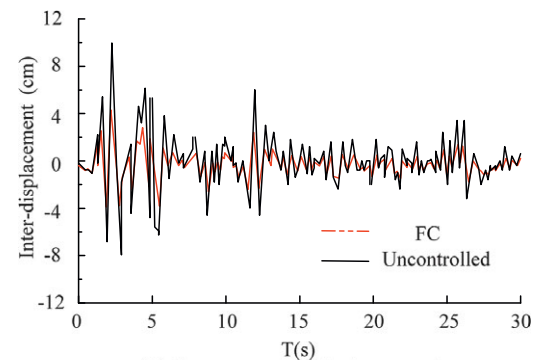
(b) Fuzzy control of displacement time history curve between lower layers

Figure 11. Time history results of interlayer displacement of the top layer under different control strategies under the action of Centro seismic waves.

Figure 9 (a) shows the acceleration time history results of EI seismic wave. From the curve results, the acceleration time history remained high within 5 seconds before the earthquake and gradually decreased thereafter. Figure 9 (b) shows the acceleration time history results of Kobe seismic wave. According to the curve results, the acceleration time history value was low in the first 5 s, increased in 7 to 13 s, then gradually decreased, and the seismic fluctuation gradually decreased. Figure 10 shows the relationship between SC force, interlayer displacement, and seismic acceleration.

In Figure 10, the relationship between interlayer displacement, seismic acceleration, and control force was obtained through simulation experiments. When the acceleration was 5 m/s² and the interlayer displacement was 5 cm, both the acceleration and interlayer displacement corresponded to the NB level, which was the most unfavorable state for SC and needed to exceed 15 n/m². Seismic acceleration was negatively correlated with ISD, and as the displacement and seismic acceleration increased, the risk of concrete structures gradually increased. The interlayer displacement curves under different control strategies are shown in Figure 11.

Figure 11 (a) shows the displacement results between the top floors under LQR control. From the data results, in uncontrolled concrete structures, as the seismic excitation time increased, the interlayer displacement gradually decreased and tended to stabilize. At the second of seismic excitation, the maximum displacement value achieved by uncontrolled structural interlayer displacement was 9 cm. Using traditional LQR SC, the interlayer displacement was 5 cm at the second. Compared with uncontrolled control, LQR SC could effectively suppress the interlayer displacement caused by seismic excitation. Figure 11 (b) shows the displacement results
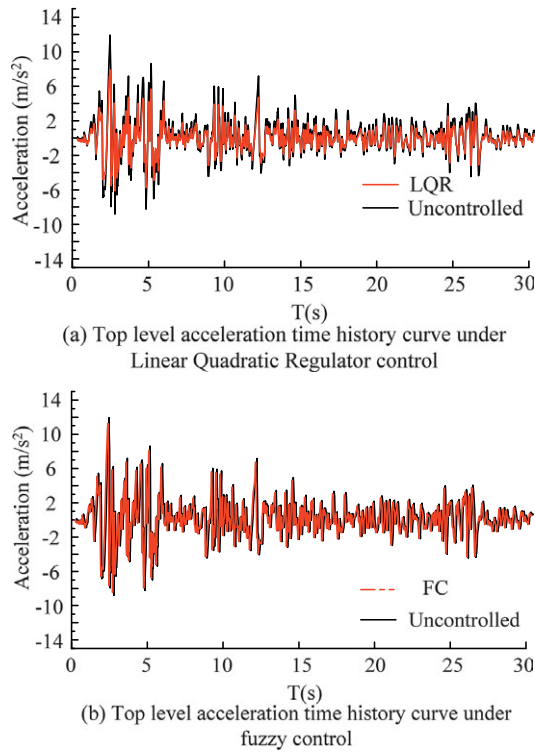
Figure 12. Acceleration time history results of top floor buildings under different control strategies under the action of Centro seismic waves.

Figure 13. The time history results of ISD of the lower concrete structure.

between the top floors under FC. At the second, fifth, and 14th seconds of seismic excitation, there was significant ISD in the uncontrolled structure, with displacement amounts of 9, 7, and 6 cm, respectively. In FC, the displacement amounts were 4, 2, and 2 cm, respectively. By comparing two SC technologies, FC has improved interlayer displacement control by 21.36% compared to LQR. The acceleration curves under different control strategies are shown in Figure 12.

Under seismic excitation, it was also necessary to consider the impact on building acceleration. Figure 12 (a) and 12 (b) shows the acceleration time history curves of the top floor of the building under LQR control and FC, respectively. In Figure 12 (a), during the first 5 seconds of seismic excitation, the building model was subjected to the strongest seismic force. In the uncontrolled structure, the maximum acceleration value of -14 m/s^2 occurred in the third second. In the LQR SC, the vibration of the concrete structure was suppressed, and in the third second, the building acceleration was -5 m/s^2. In Figure 11 (b), FC strategy 1 was selected for the experiment. The floor acceleration under it was higher than that under LQR control, but the forces between different floors were effectively suppressed, which had a lower impact on seismic effects compared to LQR control. It studied the ISD of the top 20 concrete structure, as shown in Figure 13.

Figure 13 (a) shows the acceleration time history curve results of the top floor of the building under LQR control. From the data results, the max interlayer displacement value of -12 cm occurred in the uncontrolled lower floor of the building at the 9th second of seismic excitation. Under LQR control, the maximum interlayer displacement value was -7 cm at the 9th second, and 3 cm, −6 cm, and 3 cm at the 10th, 11th, and 12th seconds, respectively. Compared with no control, the interlayer displacement of the lower layer of the building was suppressed, and the interlayer displacement
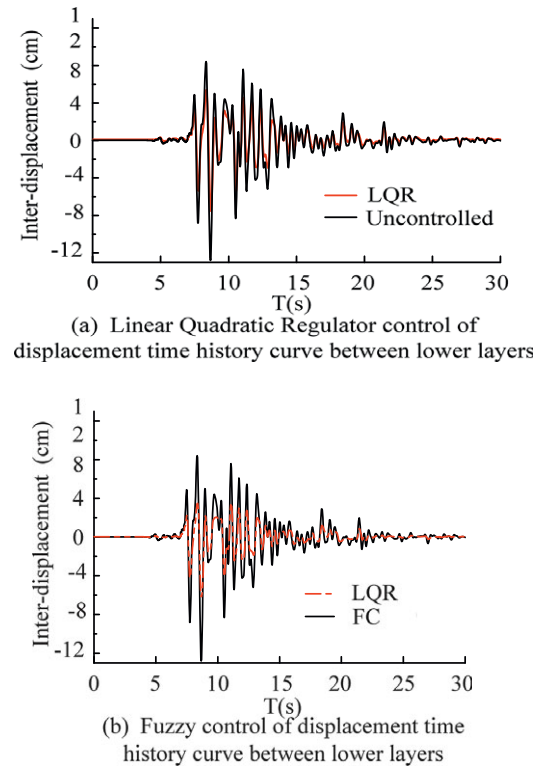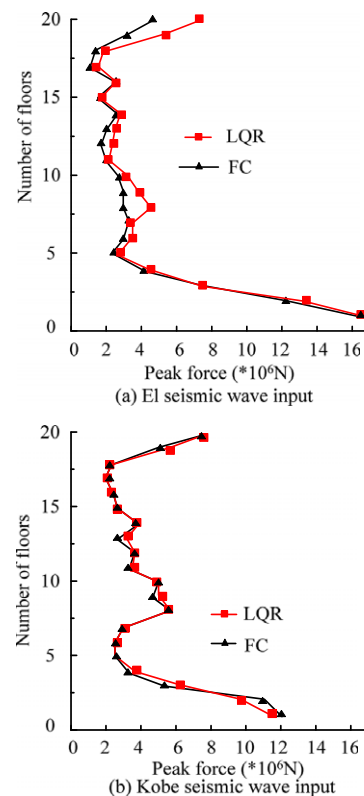

Figure 14. Control force results between layers.

decreased by 46.65% compared to no control. Figure 13 (b) shows the acceleration time history curve results of the lower floor of the building under FC. From the data results, the max interlayer displacement value without control was -7 cm at 9 s, and at this moment, while the value under FC was −6. At 10, 11, and 12 s, the interlayer displacement values were 3, −5, and 3 cm, respectively. Compared with LQR control, FC had better suppression of interlayer displacement, with a reduction of 51.32% compared to no control. FC had a better effect in the vibration control of HRBs. Simultaneously the control forces between each layer were compared, as shown in Figure 14.

Figure 14 (a) shows the control effect of each layer under EI seismic wave. From the Figure, there was a certain difference in the control force between FC and LQR control in each floor of HRBs. From the zeroth floor to the fifth floor, the two types of SC had basically the same control force in each floor. At the seventh and eighth floors, due to different SC methods, FC required significantly lower floor control force compared to LQR control. At the seventh floor, the LOR control floor control force was 4.7×106 N, while the FC floor control force required at the seventh floor was 2.4×106 N. The FC floor control effect was improved by 32.65% compared to LQR control floor control. Figure 13 (b) shows the control effect of each layer under the Kobe seismic wave. According to the data in the figure, under the effect of the Kobe seismic wave, the floor control forces of LOR control and FC were basically the same. However, on the third floor, the floor control forces required by LQR control and FC were 10.0×106 N and 11.6×106 N, respectively. The possible reason was that the FC adopted sectional control to ensure the stability of the floor earthquake resistance. Compared with LOR control, the floor control effect of FC was increased by 11.56%.

Results of proposed multifloor fuzzy decentralized control

The same seismic excitation was selected as in Section "Concrete structure based on fuzzy DC" for testing, and a 6-story shear-type building model was utilized as the experimental object. Each floor had a height of 3.4 m and a stiffness value of 12000 KN/m. The peak control force of concrete structures under seismic excitation is shown in Table 3.

Table 3 shows the peak control force results of concrete structures under seismic excitation. In the control of multilayer structures, MRFD and FC were installed in each floor to ensure the control effect of lateral displacement of the floors. From Table 3, there were significant differences in the SC effects among the three types of SCs in multifloor SC. In FC, MRFDs were installed on each

floor to reduce lateral forces. In the comparison of lateral displacement, the total lateral displacement without control was 92.65 cm, LQR control was 47.03 cm, and FC was 49.95 cm. Overall, FC dynamically adjusted lateral effects and had the best stability among the three. At the same time, in the comparison of acceleration peaks, the total acceleration peak of FC was 36.65 m/s^2, and the LQR control was 34.55 m/s^2. Due to the placement of MRFDs in different floors of FC, the building acceleration was effectively controlled. In the comparison of control forces, the total control force of the six layers under LQR control was 741 KN, while the FC was 718 KN. FC had better control effects. At the same time, in actual building SC, it was also necessary to consider the impact of output variables on SC, including open-loop control with seismic acceleration as input, closed-loop control with floor acceleration and displacement as input, and closed-loop open control with seismic acceleration and displacement as input.

At the same time, under open-loop control, the optimal building displacement control effect was achieved on the 6th floor, with a displacement of 7.9 m/s^2 on the top floor. From this, reasonable control parameters needed to be selected in practical control to achieve the best control effect. Figure 15 shows the convergence of the desired response under control force. Finally, a 12-story reinforced concrete structure was selected to test the application effect of the proposed technology in practical scenarios. The structural parameters of the building are shown in Table 4.

The actual application effect of the proposed technology was evaluated by introducing three indicators: maximum acceleration damping rate J1, top displacement damping rate J2, and MRFD damping maximum output J3, as shown in Table 5.

From the data in Table 5, the proposed FC strategy greatly reduced the acceleration and displacement response of the structure under wind load, and was superior to the IQR control strategy, especially in terms of acceleration damping rate J1 control, which was 0.03546, while the LQR was 0.03934. At the same time, FC had a better overall effect in controlling the top displacement damping rate J2 and MRFD damping maximum output J3. In addition, in comprehensive comparison, the proposed FC technology did not damage the concrete structure, while the other two methods both had certain structural damage. The proposed technology had better application effects and met the SC requirements of actual earthquake scenarios in buildings.

Conclusions and discussions

In recent years, the number of HRBs has been increasing, and the seismic risk faced by their structures has also been increasing. In the

Table 3. Peak control force of concrete structures under seismic excitation

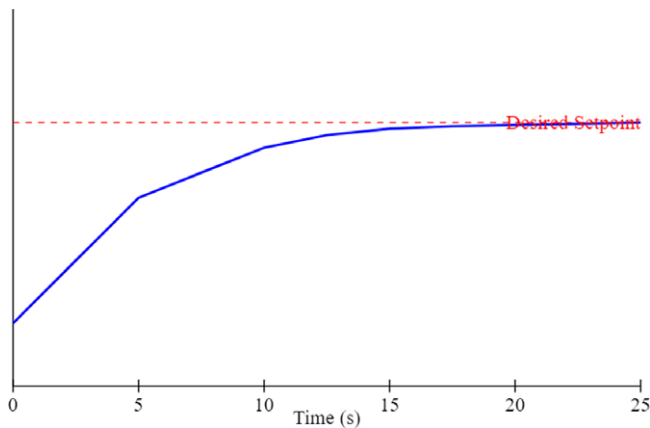| Number of layers		1	2	3	4	5	6	Sum of 6 layers
Lateral displacement (cm)	Uncontrolled	5.2	10.22	14.82	18.64	21.63	23.46	92.65
	LQR	2.7	5.2	7.44	9.36	10.83	11.64	47.03
	FC	3.09	5.95	7.59	10.04	11.07	12.21	49.95
Peak acceleration (m/s^2)	Uncontrolled	6.6	7.8	8.7	8.53	9.64	11.86	53.13
	LQR	5.24	6.18	5.29	5.74	7.06	7.9	36.65
	FC	4.64	6.64	4.64	5.64	6.54	6.45	34.55
Control force (KN)	LQR	175	164	146	120	89	48	741
	FC	166	158	144	118	84	48	718

Figure 15. the system response indicated by the red dashed line.

Table 4. Structural parameters of actual building scenarios

Number of layers	1	2 ~ 11	12
Weight (kg)	9. 86 × 104	8.574	6.615
Stiffness (kN·m)	4.3 × 104	8.1 × 104	8.1 × 104

Table 5. Comparison of control effects in three actual control scenarios

Performance index	FC	Uncontrolled	LQR
J1	0.03546	0.07568	0.03934
J2	0.97440	0. 97580	0.96490
J3	0.48154	1.20000	0.43107
Comprehensive control effect	Structural safety and small displacement	Severe displacement, structural damage	Minor structural damage, slight movement

field of construction engineering, centralized control is often used, and damage to control units can have an impact on the entire control system. For the SCs of buildings in vibration scenarios, decentralized control technology is introduced and FC algorithms are used to solve this problem. Firstly, the semiactive control problem of 20-story buildings affected by earthquakes is studied, and fuzzy strategy is introduced to improve the accuracy of traditional control algorithms. Taking into account the shortcomings of centralized control in a 20-story building, a new controller is designed using FC and DC strategies to optimize the problem. For the problem of SCs failure in multistory buildings affected by earthquakes, a dual-drive damper installation strategy is introduced to design SCs units that meet the control requirements of multistory buildings. In the fuzzy DC test, Centro seismic wave is selected to verify the control effect of FC and LQR. The LQR structure controls an interlayer displacement of 5 cm in the second, and an FC of 4 cm. The FC improves the interlayer displacement control by 21.36% compared to the LQR. In the comparison of multistory buildings, the total acceleration peak of FC is 36.65 m/s^2, and the LQR control is 34.55 m/s^2. FC has a better control effect on building acceleration. In the comparison of control forces, the minimum total control force of FC for the sixth-story building is 718KN, which is better

than the control effect of LQR. The research content provides important technical references for the safety design and seismic optimization of HRB structures.

Designing and building HRBs using FC combined with LQR techniques offers several significant advantages and impacts. The combination of FC and LQR allows for real-time adjustments to control inputs based on the current state of the building, improving its ability to respond to earthquakes. The significance of using FC combined with LQR in designing and building HRBs lies in its ability to enhance control performance, improve structural stability, and ensure occupant safety and comfort. This hybrid approach not only addresses the complexities of modern building dynamics but also promotes cost-effectiveness and adaptability in an ever-changing environment. As urbanization continues to rise, these advancements will play a crucial role in the future of high-rise construction and management.

Reference

Cai G, **Zheng X**, **Gao W and Guo J** (2024) Self-extinction characteristics of fire extinguishing induced by nitrogen injection rescue in an enclosed urban utility tunnel. *Case Studies in Thermal Engineering* **59**, 104478. https://doi.org/10.1016/j.csite.2024.104478.

Chen ZY, **Meng YH**, **Wang RY** (2024a) "A novel recurrent self-evolving fuzzy neural network for consensus decisionmaking of unmanned aerial vehicles". *International Journal of Advanced Robotic Systems* **21**(2), 1–14.

Chen ZY, **Meng YH**, **Wang RY** (2024b) "Neural ordinary differential grey algorithm to forecasting MEVW systems". *International Journal of Computers Communications & Control* **19**(1), 4676. https://doi.org/10.15837/ijccc.2024.1.4676.

Chen ZY, **Meng YH**, **Wang RY** (2024c) "Optimal design via polynomial Euler function for UAV applications". *Journal of Navigation*, Published online 1–18. https://doi.org/10.1017/S0373463324000146.

Chen H, **Huang B**, **Zhang H**, **Xue K**, **Sun M and Wu Z** (2024d) An efficient Bayesian method with intrusive homotopy surrogate model for stochastic model updating. *Computer-Aided Civil and Infrastructure Engineering* **39**(16), 2500–2516. https://doi.org/10.1111/mice.13206.

Fu L, **Guo J**, **Shen W**, **Wang X**, **Liu X**, **Chen X and Hu X** (2024) Geophysical evidence of the collisional suture zone in the Prydz Bay, East Antarctica. *Geophysical Research Letters* **51**(2), e2023GL106229. https://doi.org/10.1029/2023GL106229.

Gao N, **Zeng Y**, **Wang J**, **Wu D**, **Zhang C**, **Song Q and Jin S** (2021) Energy model for UAV communications: Experimental validation and model generalization. *China Communications* **18**(7), 253–264. https://doi.org/10.23919/JCC.2021.07.020.

Gong B and Li H (2024) A couple Voronoi-RBSM modeling strategy for RC structures. *Structural Engineering and Mechanics* **91**(3), 239–250. https://doi.org/10.12989/sem.2024.91.3.239.

Guo C, **Hu J**, **Hao J**, **Čelikovský S, and Hu X** (2023) "Fixed-time safe tracking control of uncertain high-order nonlinear pure-feedback systems via unified transformation functions". *Kybernetika* **59**(3), 342–364. https://doi.org/10.14736/kyb-2023-3-0342

Hu H, **Qi L and Chao X** (2024) Physics-informed neural networks (PINN) for computational solid mechanics: Numerical frameworks and applications. *Thin-Walled Structures* **205**, 112495. https://doi.org/10.1016/j.tws.2024.112495.

Huang H, **Chen Z**, **Zhao M**, **Wang B and Ye Y** (2024) Seismic performance of frame with middle partially encased composite brace and steel-hollow core partially encased composite spliced frame beam. *Journal of Building Engineering* **95**, 110226. https://doi.org/10.1016/j.jobe.2024.110226.

Huang H, **Guo M**, **Zhang W and Huang M** (2022) Seismic behavior of strengthened RCCol umns under combined loadings. *Journal of Bridge Engineering* **27**(6). https://doi.org/10.1061/(ASCE)BE.1943-5592.0001871.

Li J, **Hu Z**, **Cui J and Lin G** (2024) Efficient GPU-accelerated seismic analysis strategy and scenario simulation for large-scale nuclear structure cluster-soil interaction over ten million DOFs. *Computers and Geotechnics* **174**, 106583. https://doi.org/10.1016/j.compgeo.2024.106583.

Liu Y, **Jiang D**, **Yun J**, **Sun Y**, **Li C**, **Jiang G**, **Kong J**, **Tao B and Fang Z** (2022) "Self-Tuning Control of Manipulator Positioning Based on Fuzzy PID and PSO Algorithm". *Front. Bioeng. Biotechnol.* **9**, 817723. https://doi.org/10.3389/fbioe.2021.817723

Long S, **Huang W**, **Wang J**, **Liu J**, **Gu Y and Wang Z** (2024a) A fixed-time consensus control with prescribed performance for multi-agent systems under full-state constraints. *IEEE Transactions on Automation Science and Engineering* 1–10. https://doi.org/10.1109/TASE.2024.3445135.

Long X, **Li H**, **Iyela PM and Kang S** (2024b) Predicting the bond stress–slip behavior of steel reinforcement in concrete under static and dynamic loadings by finite element, deep learning and analytical methods. *Engineering Failure Analysis* **161**, 108312. https://doi.org/10.1016/j.engfailanal.2024.108312.

Lu LT, et al. (2003) Active control for a benchmark building under wind excitations. *Journal of Wind Engineering and Industrial Aerodynamics* **91**, 4, 469–493, https://doi.org/10.1016/S0167-6105(02)00431-2.

Qi H, **Zhou Z**, **Irizarry J**, **Deng X**, **Yang Y**, **Li N and Zhou J** (2024) Modification of HFACS model for path identification of causal factors of collapse accidents in the construction industry. *Engineering, Construction and Architectural Management*. https://doi.org/10.1108/ECAM-02-2023-0101.

Shu J, **Yu H**, **Liu G**, **Duan Y**, **Hu H and Zhang H** (2025) DF-C DM: Conditional diffusion model with data fusion for structural dynamic response reconstruction. *Mechanical Systems and Signal Processing* **222**, 111783. https://doi.org/10.1016/j.ymssp.2024.111783.

Sun R, **Wang S**, **Li M and Zhu Y** (2025) An algorithm for large-span flexible bridge pose estimation and multi-keypoint vibration displacement measurement. *Measurement* **240**, 115582. https://doi.org/10.1016/j.measurement.2024.115582.

Tai S, **Bu C**, **Wang Y**, **Yue T**, **Liu H and Wang L** (2024) Identification of aircraft longitudinal aerodynamic parameters using an online correctivetest for wind tunnel virtual flight. *Chinese Journal of Aeronautics* **37**(9), 261–275. https://doi.org/10.1016/j.cja.2024.05.031.

Tang H and Zhu M (2025) A nonlinear breakage mechanics model: From extreme entire life model to breakage evolution of limestone based on separation of Helmholtz free energy under cyclic loading. *International Journal of Geomechanics* **25**(2), 4024336. https://doi.org/10.1061/IJGNAI.GMENG-10244.

Wang J, **Bai L**, **Fang Z**, **Han R**, **Wang, J and Choi J** (2024a) Age of information based URLLC transmission for UAVs on pylon turn. *IEEE Transactions on Vehicular Technology* **73**(6), 8797–8809. https://doi.org/10.1109/TVT.2024.3358844.

Wang K, **Cao J**, **Ye J**, **Qiu Z and Wang X** (2024b) Discrete element analysis of geosynthetic-reinforced pile-supported embankments. *Construction and Building Materials* **449**, 138448. https://doi.org/10.1016/j.conbuildmat.2024.138448.

Wang M, **Kang J**, **Liu W**, **Li M**, **Su J**, **Fang Z and Guo C** (2024d) Design and study of mine silo drainage method based on fuzzy control and avoiding peak filling valley strategy. *Scientific Reports* **14**(1), 9300. https://doi.org/10.1038/s41598-024-60228-x.

Wang S, **Lin S and Yang R** (2024f) A lightweight convolutional neural network for multipoint displacement measurements on bridge structures. *Nonlinear Dynamics* **112**(14), 11745–11763. https://doi.org/10.1007/s11071-024-09673-x.

Wang J, **Wu Y**, **Chen CLP**, **Liu Z and Wu W** (2024h) Adaptive PI event-triggered control for MIMO nonlinear systems with input delay. *Information Sciences* **677**, 120817. https://doi.org/10.1016/j.ins.2024.120817.

Wang K, **Ye J**, **Wang X and Qiu Z** (2024i) The soil-arching effect in pile-supported embankments: A review. *Buildings* **14**(1), 126. https://doi.org/10.3390/buildings14010126.

Wang J, **Zhang Y**, **Wang K**, **Li L**, **Cheng S and Sun S** (2024k) Development of similar materials with different tension-compression ratios and evaluation of TBM excavation. *Bulletin of Engineering Geology and the Environment* **83**(5), 190. https://doi.org/10.1007/s10064-024-03674-1.

Wang L, **She A, and Xie Y** (2023) "The dynamics analysis of Gompertz virus disease model under impulsive control". *Scientific Reports*, **13**(1), 10180. https://doi.org/10.1038/s41598-023-37205-x

Wu Y, **Fan Y**, **Zhou S**, **Wang X**, **Chen, Q and Li X** (2024) Research on the cross-sectional geometric parameters and rigid skeleton length of reinforced concrete arch bridges: A case study of Yelanghu bridge. *Structure* **69**, 107423. https://doi.org/10.1016/j.istruc.2024.107423

Xie M, **Xu F**, **Wang Z**, **Yin LE**, **Wu X**, **Xu M and Li X** (2025) Investigating fire collapse early warning Systems for Portal Frames. *Buildings* **15**(2), 296. https://doi.org/10.3390/buildings15020296.

Xu D, **Zhang S and Qin Y** (2024) Study of the micromechanical properties and dissolution characteristics of porous coral reef limestone. *Journal of Geophysical Research: Solid Earth* **129**(11), e2024JB029131. https://doi.org/10.1029/2024JB029131.

Xu B, **Wang X**, **Zhang J**, **Guo Y, and Razzaqi AA** (2022) "A novel adaptive filtering for cooperative localization under compass failure and non-gaussian noise". *IEEE Transactions on Vehicular Technology* **71**(4), 3737–3749. https://doi.org/10.1109/TVT.2022.3145095

Xu G, **Guo T**, **Li A**, **Zhou T and Shuang C** (2025a) Seismic performance of steel frame structures with novel self-centering beams: Shaking-table tests and numerical analysis. *Journal of Structural Engineering* **151**(3), 4025002. https://doi.org/10.1061/JSENDH.STENG-13516.

Xu Z, **Zhu Y**, **Fan J**, **Zhou Q**, **Gu D and Tian Y** (2025b) A spatiotemporal casualty assessment method caused by earthquake falling debris of building clusters considering human emergency behaviors. *International Journal of Disaster Risk Reduction* **117**, 105206. https://doi.org/10.1016/j.ijdrr.2025.105206.

Yang L, **Gao Y**, **Chen H**, **Jiao H**, **Dong M**, **Bier TA and Kim M** (2024a) Three-dimensional concrete printing technology from a rheology perspective: A review. *Advances in Cement Research* **36**(12), 567–586. https://doi.org/10.1680/jadcr.23.00205.

Yang Q, **Li H**, **Zhang L**, **Guo K and Li K** (2024b) Nonlinear flutter in a wind-excited double-deck truss girder bridge: Experimental investigation and modeling approach. *Nonlinear Dynamics*. https://doi.org/10.1007/s11071-024-10496-z.

Yang Q, **Zeng X**, **Guo K**, **Cao S**, **Wei K**, **Shan W and Tamura Y** (2025) Analysis of vortex-induced vibration in flexible risers using a physically-meaningful wake-oscillator model. *Engineering Structures* **325**, 119415. https://doi.org/10.1016/j.engstruct.2024.119415.

Yao Y, **Huang H**, **Zhang W**, **Ye Y**, **Xin L and Liu Y** (2022) Seismic performance of steel-PEC spliced frame beam. *Journal of Constructional Steel Research* **197**, 107456. https://doi.org/10.1016/j.jcsr.2022.107456.

Zhang C, **Duan C and Sun L** (2024a) Inter-Storey isolation Versus Base isolation using friction pendulum systems. *International Journal of Structural Stability and Dynamics* **24**(2), 2450022. https://doi.org/10.1142/S0219455424500226.

Zhang W, **Lin J**, **Huang Y**, **Lin B and Liu X** (2024b) Experimental and numerical studies on flexural performance of composite beams under cyclic loading. *Structure* **70**, 107728. https://doi.org/10.1016/j.istruc.2024.10772.

Zhang C, **Liu M**, **Mohammadzadeh A and Taghavifar H** (2024c) A fractional adaptive type-2 fuzzy structural control system: Theoretical/experimental study. *Structure* **70**, 107843. https://doi.org/10.1016/j.istruc.2024.107843.

Zhang C, **Shu J**, **Zhang H**, **Ning Y and Yu Y** (2024e) Estimation of load-carrying capacity of cracked RC beams using 3D digital twin model integrated with point clouds and images. *Engineering Structures* **310**, 118126. https://doi.org/10.1016/j.engstruct.2024.118126.

Zhou X, **Lu D**, **Zhang Y**, **Du X and Rabczuk T** (2022) An open-source unconstrained stress updating algorithm for the modified cam-clay model. *Computer Methods in Applied Mechanics and Engineering* **390**, 114356. https://doi.org/10.1016/j.cma.2021.114356.

Zhou Z, **Zhuo W**, **Cui J**, **Luan H**, **Chen Y and Lin D** (2025) Developing a deep reinforcement learning model for safety risk prediction at subway construction sites. *Reliability Engineering & System Safety* **257**, 110885. https://doi.org/10.1016/j.ress.2025.110885.